JCAMECH

Vol. 50, No. 1, June 2019, pp 14-26
DOI:10.2205910.22059/JCAMECH.2018.248898.224

Hydrodynamic Investigation of Multiple Rising Bubbles Using Lattice Boltzmann Method

Mohsen Ghasemi[a], Mohammad Reza Ansari[a,], Mohammad Hasan Rahimian[b]*

[a] *Department of Mechanical Engineering, Tarbiat Modares University, Tehran, Iran.*
[b] *Department of Mechanical Engineering, University of Tehran, Tehran, Iran*

ARTICLE INFO

Article history:
Received 31 December 2017
Accepted 06 April 2018
Available online 25 April 2018

Keywords:
Multiple rising bubbles
Lattice Boltzmann method
Lee two-phase model

ABSTRACT

Hydrodynamics of multiple rising bubbles as a fundamental two-phase phenomenon is studied numerically by lattice Boltzmann method and using Lee two-phase model. Lee model based on Cahn-Hilliard diffuse interface approach uses potential form of intermolecular forces and isotropic finite difference discretization. This approach is able to avoid parasitic currents and leads to a stable procedure to simulate two-phase flows. Deformation and coalescence of bubbles depend on a balance between surface tension forces, gravity forces, inertia forces and viscous forces. A simulation code is developed and validated by analysis of some basic problems such as bubble relaxation, merging bubbles, merging droplets and single rising bubble. Also, the results of two rising bubbles as the simplest interaction problem of rising bubbles have been calculated and presented. As the main results, square and lozenge initial configuration of nine rising bubbles are studied at Eotvos numbers of 2, 10 and 50. Two-phase flow behavior of multiple rising bubbles at same configurations is discussed and the effect of Eotvos number is also presented. Finally, velocity field of nine rising bubbles is presented and discussed with details.

1. Introduction

In many industrial equipments, such as steam generators in nuclear and fossil power plants, condensers, and boilers, there are two phases of fluids, the liquid and the gas phase, flowing simultaneously. Understanding of two-phase flow dynamics is therefore of great importance in design, analysis and maintenance of these types of equipments.

Among two-phase flow problems, motion of rising bubbles due to gravity force is one of the most important and complicated phenomena, which exact understanding of its dynamics and accurate simulation of the interface forces, can be useful for a better design and development of the corresponding industrial equipments. Hence, dynamics of rising bubble is one of the most important topics in many experimental and numerical researches. Clift et al [1] conducted an experiment and derived some correlations, which was reviewed and modified later by Bhaga and Weber [2]. Motion of a rising bubble in viscous liquid due to gravity can be classified into several regimes. A chart of bubble shapes known as Grace diagram, is shown in Fig. 1 (Grace et al [3]).

As Figure 1 shows, bubble shape is determined by two important non-dimensional numbers called Eotvos (Eo) or Bond (Bo) and Morton (Mo), which are defined as follows:

$$\mathrm{Eo} = \mathrm{Bo} = \frac{g\Delta\rho d_0^2}{\sigma} \tag{1}$$

$$\mathrm{Mo} = \frac{g\Delta\rho\mu_l^2}{\sigma^3\rho_l^4} \tag{2}$$

In the above equations, g is the gravitational acceleration, d_0 is the initial diameter of bubble, σ is surface tension, μ_l and ρ_l are liquid viscosity and density, respectively and $\Delta\rho$ is the density difference between liquid and gas phases.

Moreover, interaction of multiple bubbles is of a particular interest for two-phase flow researchers, where many studies are conducted on this subject. Some recent researches have been performed by Watanabe et al [4], Balcázar et al [5], Islam [6], who used Molecular Dynamics (MD) method, Level Set (LS) method, and Volume of Fluid (VOF) technique, respectively, to simulate and study the interaction dynamics of two bubbles.

Lattice Boltzmann Equation (LBE) methods have also a desirable capability to simulate fluid dynamics and have acquired an increasing growth during recent decades. Various problems of fluid dynamics such as unsteady flows, phase separation, evaporation and condensation, cavitation, heat transfer, and also fluid-surface interaction problems can be simulated using lattice Boltzmann models. As some recent studies, researches of Hassanzadeh et al [7-8], Ghafouri and Hassanzadeh [9] and Dadvand [10-11] can be mentioned.

Nomenclature

Bo	Bond number
C	concentration (or composition variable)
D	interface thickness
c_s	lattice sound speed
d_0	initial diameter of bubble
Eo	Eotvos number
E_0	bulk energy
e_α	particle speed
F	force term
F_{ext}	external force (gravitational force)
f_α	particle distribution function
f_α^{eq}	equilibrium particle distribution function
g	gravitational acceleration
g_α	pressure distribution function
$\bar{g}_\alpha$	modified pressure distribution function
h_α	composition distribution function
$\bar{h}_\alpha$	modified composition distribution function
lu	lattice length unit
M	mobility
Mo	Morton number
mu	lattice mass unit
p_1	hydrodynamic pressure
T	lattice time
$\bar{T}$	specific time
T^*	non-dimensional time
t	time
tu	Lattice time unit
u	Velocity
$\Delta\rho$	density difference
λ	relaxation time
μ	chemical potential
μ_l	liquid viscosity
ρ_g	gas density
ρ_l	liquid density
σ	surface tension
τ	non-dimensional relaxation time

There are several lattice Boltzmann models for two-phase flow simulation; in 1990s, the first decade of multiphase lattice Boltzmann methods application, several models were introduced, usually classified into four categories of chromodynamic models (Gunstensen et al [12], Grunau et al [13]), pseudo-potential models (Shan and Chen [14-15], Shan and Doolen [16-17]), free energy models (Swift et al [18-19], Orlandini et al [20]) and models based on inter-molecular interaction (He et al [21-23], Zhang et al [24-25], Zhang [26]).

Attempts continued in the next decade (2000s) to develop two-phase lattice Boltzmann models and to achieve higher density ratios. Of such studies, models developed by Inamuro et al [27], Lee and Lin [28] and Zheng et al [29] can be mentioned.

Dynamics of multiple bubble interaction has also been studied in the past by different researches. Takada et al [30] used a model developed based on free energy method and simulated motion of one and two rising bubbles. Their results complied with the VOF simulated results and they managed to simulate the behavior of two merging bubbles.

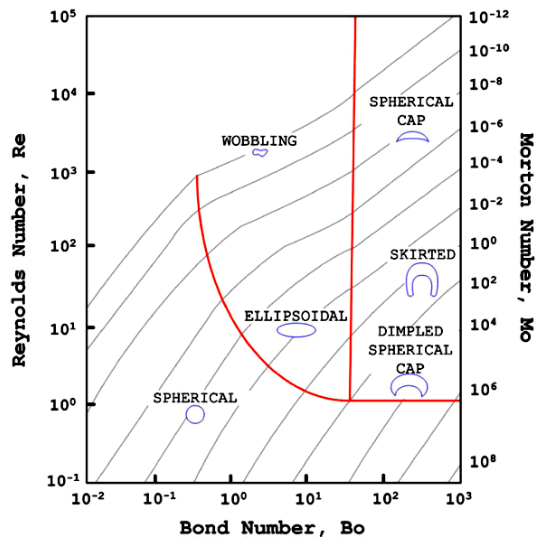

Figure 1. Diagram of bubble shapes at various regimes

Gapta and Kumar [31] simulated the motion of two and three bubbles due to gravity using a potential model. They simulated two linear and staggered alignments of bubbles and showed that with an increase in Eotvos number, the former bubble undergoes larger deformations and due to the wake behind, the bubbles merge finally.

Based on free energy model, Cheng et al [32] developed a model to simulate bubble-bubble interaction and studied the effect of density ratio and initial bubble configuration on flow field and coalescence of bubbles. They showed that in the two bubble configuration with the same diameter, while the former bubble behaves as an isolated bubble before merging, the trailing bubble is entrained by the leading one and experiences obvious deformation as it enters the wake region of the leading one. The shape evolution of the trailing bubble is different for high and low density ratios. However, for two rising bubbles with different sizes, the larger bubble always has a strong effect over the smaller one for any initial configuration.

Yu et al [33] developed an adaptive lattice Boltzmann model to simulate a pair of bubbles with spherical or ellipsoidal shapes under different configurations and rise velocities. It was shown that both attractive and repulsive interactions can be observed in the simulations depending on the relative position and the Reynolds number. They also simulated a group of 14 bubbles and investigated the effects of the bubble shape and Reynolds number on the spatial distribution of the bubbles.

Shu and Yang [34] used a lattice Boltzmann method to solve the phase-field model and could accurately capture the interface evolution under different flow conditions and simulated the behavior of a single bubble, a bubble pair, and a bubble swarm.

One of the strongest lattice Boltzmann two-phase models is Lee model. Lee and Lin [28] proposed their two-phase model in 2005 with complete discretization and validation for the first time. In 2006, Lee and Fischer [35] studied the elimination of parasitic current in Lee model. Yet, wall boundary condition was not considered in the model. In 2008, Lee and Liu [36] examined wall boundary condition in Lee model. The LBE simulations of the contact line are typically contaminated by small but strong counter-rotating parasitic currents near solid surfaces. They found that these currents can be eliminated to round-off if the potential form of the intermolecular force is used with the boundary conditions based on the wall energy approach and the bounce-back rule. In 2009, Lee [37] investigated the effects of incompressibility on the elimination of parasitic currents in his model. In 2010, Lee and Lin [38] presented a better expression of Lee model and simulated a droplet impact to a solid surface. In 2010 and 2011, Amaya-Bower and Lee [39-40] considered the gravity force in the Lee model for the first time. Later on, Lee model was developed, extended, and applied to various two-phase problems by other researches such as Taghilou and Rahimian [41], Mirzaie Daryan and Rahimian [42], Haghani and Rahimian [43], Farokhirad et al [44], and Fakhari et al [45].

In the present paper, motion dynamics of a nine bubble group under the effect of gravity is investigated by Lee model for the first time. For this aim, after validation of the developed code with some standard problems, several results of multiple bubble dynamics are presented and discussed.

2. Modeling

2.1. Two-phase Lattice Boltzmann Equations

Discrete Boltzmann equation with force term takes the following form (He et al [21]):

$$\frac{Df_\alpha}{Dt} = \left(\frac{\partial}{\partial t} + e_\alpha.\nabla\right) f_\alpha = -\frac{1}{\lambda}\left(f_\alpha - f_\alpha^{eq}\right) + \frac{1}{c_s^2}(e_\alpha - u).F\Gamma_\alpha \tag{3}$$

The force term is obtained by determining the non-ideal gas effects as follows:

$$F = \nabla\rho c_s^2 - \nabla p_1 - C\nabla\mu(C) + F_{ext} \tag{4}$$

with C being the concentration parameter and p_1 the hydrodynamic pressure. External force (gravitational force) is calculated from to the equation below:

$$F_{ext} = (\rho_l - \rho_g)g \tag{5}$$

where g is the gravitational acceleration and the subscript g denotes the gas phase. The thermodynamic pressure is calculated from the Legendre equation.

$$p_0 = C\frac{\partial E_0}{\partial C} - E_0 \tag{6}$$

where $E_0(C) \approx \beta C^2(C^2 - 1)$ is the bulk energy. In eq. (4), μ is the chemical potential and is calculated from $\mu = \mu_0 - \kappa\nabla^2 C$. The classical part of the chemical potential (μ_0) is the derivative of E_0 with respect to C:

$$\mu_0 = \frac{\partial E_0}{\partial C} \tag{7}$$

The parameters β and κ are related to the surface tension (σ) and the interface thickness (D) and are calculated as follows:

$$\beta = \frac{12\sigma}{D(\rho_l - \rho_g)^4} \tag{8}$$

$$\kappa = \frac{3D\sigma}{2(\rho_l - \rho_g)^2} \tag{9}$$

Lee [37] used two distribution functions g and h for the pressure and the composition evaluation equations, respectively.

$$g_\alpha = f_\alpha c_s^2 + (p_1 - \rho c_s^2)\Gamma_\alpha(0) \tag{10}$$

$$h_\alpha = \left(\frac{C}{\rho}\right) f_\alpha \tag{11}$$

where $\Gamma_\alpha(u) = f_\alpha^{eq}/\rho$. Taking a total derivate from the two above equations gives:

$$\frac{\partial g_\alpha}{\partial t} + e_\alpha\cdot\nabla g_\alpha = -\frac{1}{\lambda}\left(g_\alpha - g_\alpha^{eq}\right) + (e_\alpha - u)\cdot [\nabla\rho c_s^2(\Gamma_\alpha - \Gamma_\alpha(0)) + (-C\nabla\mu + F_{ext})\Gamma_\alpha] \tag{12}$$

$$\frac{\partial h_\alpha}{\partial t} + e_\alpha\cdot\nabla h_\alpha = -\frac{1}{\lambda}\left(h_\alpha - h_\alpha^{eq}\right) + (e_\alpha - u)\cdot \left[\nabla C - \frac{C}{\rho c_s^2}(\nabla p_1 + C\nabla\mu - F_{ext})\right]\Gamma_\alpha + \nabla\cdot(M\nabla\mu)\Gamma_\alpha \tag{13}$$

in which M is the mobility $M = 0.02/\beta$. The equilibrium distribution functions are given by:

$$g_\alpha^{eq} = t_\alpha[p_1 + \rho c_s^2(\frac{e_\alpha.u}{c_s^2} + \frac{(e_\alpha.u)^2}{2c_s^2} - \frac{(u.u)}{2c_s^2})] \tag{14}$$

$$h_\alpha^{eq} = t_\alpha C[1 + (\frac{e_\alpha.u}{c_s^2} + \frac{(e_\alpha.u)^2}{2c_s^2} - \frac{(u.u)}{2c_s^2})] \tag{15}$$

To facilitate the computation, the modified distribution functions g and h are applied [27].

$$\bar{g}_\alpha = g_\alpha + \frac{1}{2\tau}\left(g_\alpha - g_\alpha^{eq}\right) - \frac{\delta t}{2}(e_\alpha - u)\cdot [\nabla\rho c_s^2(\Gamma_\alpha - \Gamma_\alpha(0)) + (-C\nabla\mu + F_{ext})\Gamma_\alpha] \tag{16}$$

$$\bar{g}_\alpha^{eq} = g_\alpha^{eq} - \frac{\delta t}{2}(e_\alpha - u)\cdot [\nabla\rho c_s^2(\Gamma_\alpha - \Gamma_\alpha(0)) + (-C\nabla\mu + F_{ext})\Gamma_\alpha] \tag{17}$$

$$\bar{h}_\alpha = h_\alpha + \frac{1}{2\tau}\left(h_\alpha - h_\alpha^{eq}\right) - \frac{\delta t}{2}(e_\alpha - u)\cdot \left[\nabla C - \frac{C}{\rho c_s^2}(\nabla p_1 + C\nabla\mu - F_{ext})\right]\Gamma_\alpha \tag{18}$$

$$\bar{h}_\alpha^{eq} = h_\alpha^{eq} - \frac{\delta t}{2}(e_\alpha - u)\cdot \left[\nabla C - \frac{C}{\rho c_s^2}(\nabla p_1 + C\nabla\mu - F_{ext})\right]\Gamma_\alpha \tag{19}$$

By taking a second-order integration in time, the LBE for the pressure and composition equations are summarized as follows:

$$\bar{g}_\alpha(x + e_\alpha\delta t, t + \delta t) - \bar{g}_\alpha(x,t) = -\frac{1}{\tau + 0.5}\left(\bar{g}_\alpha - \bar{g}_\alpha^{eq}\right) + \delta t(e_\alpha - u)\cdot [\nabla\rho c_s^2(\Gamma_\alpha - \Gamma_\alpha(0)) + (-C\nabla\mu + F_{ext})\Gamma_\alpha]|_{(x,t)} \tag{20}$$

$$\bar{h}_\alpha(x + e_\alpha\delta t, t + \delta t) - \bar{h}_\alpha(x,t) = -\frac{1}{\tau + 0.5}\left(\bar{h}_\alpha - \bar{h}_\alpha^{eq}\right)(x,t) + \delta t(e_\alpha - u)\cdot \left[\nabla C - \frac{C}{\rho c_s^2}(\nabla p_1 + C\nabla\mu - F_{ext})\right]\Gamma_\alpha|_{(x,t)} + \delta t\nabla.(M\nabla\mu)\Gamma_\alpha|_{(x,t)} \tag{21}$$

The macroscopic variables can be calculated using the equations below:

$$C = \sum_{\alpha} \bar{h}_{\alpha} + \frac{\delta t}{2} \nabla \cdot (M \nabla \mu) \tag{22}$$

$$u = \frac{1}{\rho c_s^2} \sum_{\alpha} e_{\alpha} \bar{g}_{\alpha} - \frac{\delta t}{2} (C \nabla \mu + F_{ext}) \tag{23}$$

$$p_1 = \sum_{\alpha} \bar{g}_{\alpha} - \frac{\delta t}{2} u \cdot \nabla \rho c_s^2 \tag{24}$$

The density and relaxation time are given by:

$$\rho = C\rho_l + (1 - C)\rho_g \tag{25}$$

$$\tau = C\tau_l + (1 - C)\tau_g \tag{26}$$

Which are dependent to time and position.

2.2. Implementation

Implementation of the model is done in MATLAB software. Similar to almost all LBM codes, the present code includes the main steps shown in Figure 2 and some more details of model implementation are depicted in Figure 3. Periodic boundary condition is applied to both vertical and horizontal walls.

3. Results and Discussion

3.1. Validation

In this section, validation of our code results is performed by analysis of some standard problems such as bubble relaxation, merging of two bubbles or two droplets, and a single rising bubble.

3.2.1. Bubble Relaxation

A common test for evaluation of a two-phase flow solver is bubble or droplet relaxation. For this purpose, a square bubble with 40 lattice unit width is placed at the center of a 101×101 computational domain and is relaxed. In this problem periodic boundary condition is used and density ratio is set to 25.

Time history of bubble geometry is depicted in Figure 4. After about 5000 cycles, bubble forms a circle and preserves its circular shape.

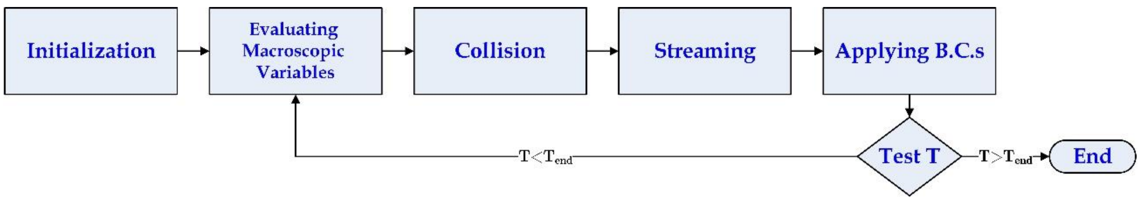

Figure 2. Main flowchart of the Present Program

Getting Input Data
Get domain and bubble data: domain length and width, diameter and initial position of bubbles
Get wall boundary flag: 0:Periodic , 1:Wall
Get $\bar{g}$ and $\bar{h}$ differentiation Method: 'CD' : Central, 'MD' : Mixed
Get fluid data: density, viscosity, surface tension
Get other data: gravitational acceleration, interface thickness, end time, export data condition, etc.

Initialization
Initialize distribution functions for all lattice nodes: $\bar{g}_{\alpha} = \bar{g}_{\alpha}^{eq}$; $\bar{h}_{\alpha} = \bar{h}_{\alpha}^{eq}$
Initialize macroscopic variables for all lattice nodes: C, u, p, μ
Calculate derivatives of macroscopic variables: ∇C , $\nabla^2 C$,$\nabla\mu$, $\nabla\rho$, ∇p, …

Repeat from T=1 to T_{end}
Evaluating Macroscopic Variables
Calculate macroscopic variables for all lattice nodes: C, u, p, μ
Calculate derivatives of macroscopic variables: ∇C, $\nabla^2 C$, $\nabla\mu$, $\nabla\rho$, ∇p, …
Collision
Calculate post-collision $\bar{g}_{\alpha}$ using Eq. 20
Calculate post-collision $\bar{h}_{\alpha}$ using Eq. 21
Streaming
Stream distribution functions: $\bar{g}$ and $\bar{h}$
Applying B.C.s
Apply periodic boundary condition at walls

Figure 3. The program pseudo-code

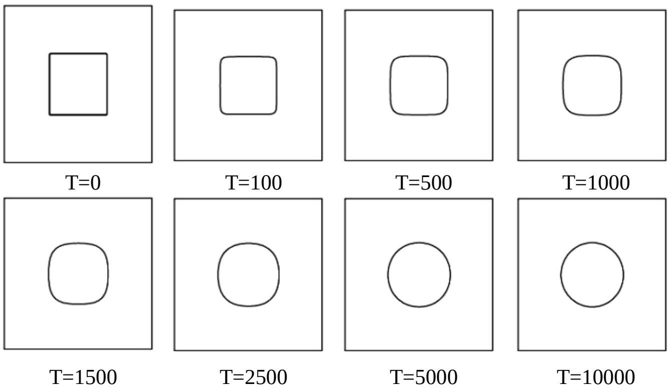

Figure 4. Time history of bubble geometry in bubble relaxation problem; $\rho_l = 1\ \frac{mu}{lu^3}$, $\rho_g = 0.04\ \frac{mu}{lu^3}$, $\mu_l = 0.167\ \frac{mu}{lu.tu}$ and $\mu_g = 0.0067\ \frac{mu}{lu.tu}$

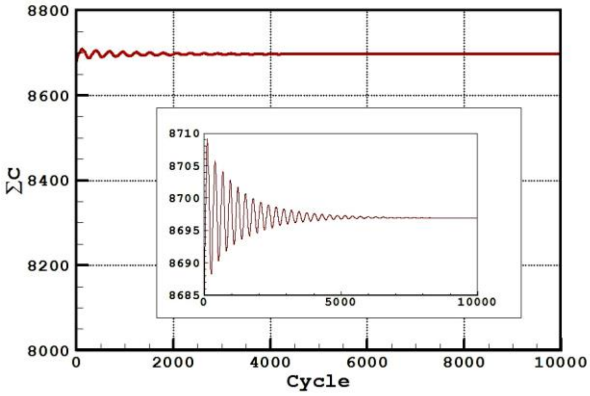

Figure 5. Summation of composition vs. time in bubble relaxation test case

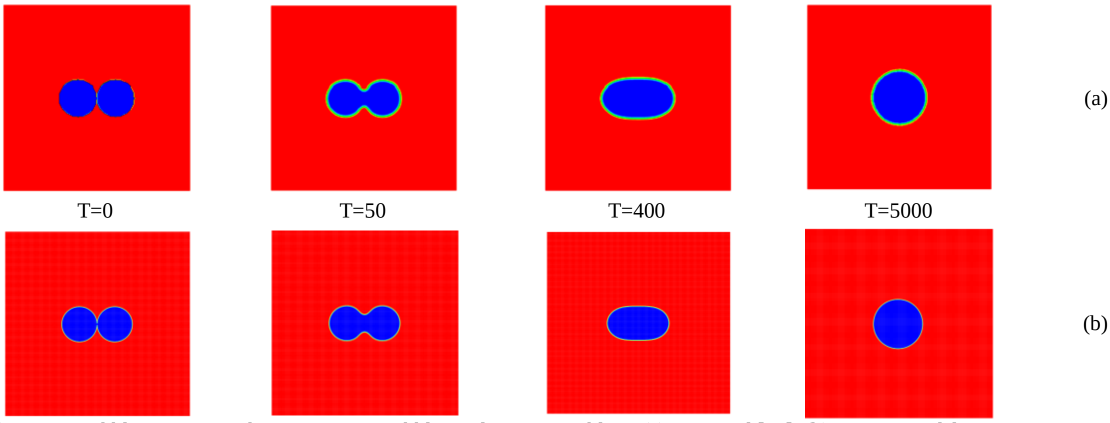

Figure. 6. Bubble Geometry Changes in Two Bubble Coalescence Problem; (a) Jain et. al.[46]; (b) Present Model

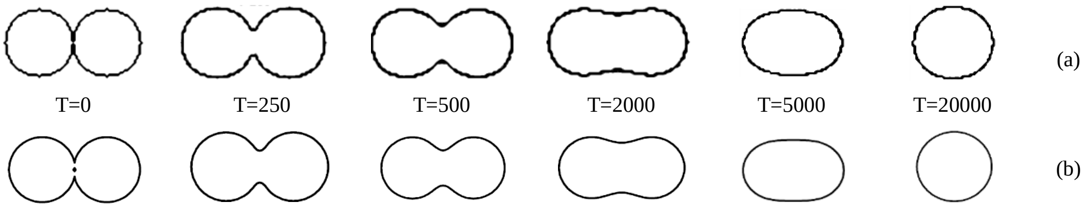

Figure 7. Droplet geometry changes in two droplet coalescence problem; (a) Xing et. al.[47]; (b) present model

Changes of summation of composition variables in time are shown in Figure 5, which demonstrates mass conservation and convergence of the model for this test case. Mass conservation errors are less than 0.1%.

3.1.2. Merging Bubbles and Droplets

More validation is conducted to prove the accuracy of the developed two-phase flow code. In this step, two merging bubbles or droplets are simulated. For this purpose, two bubbles with 38 lattice unit initial diameter are placed next to each other. Other conditions are set similar to Jain et al [46], which are 200×200 computational domain, density ratio of 40, kinematic viscosity ratio of 6.5, and periodic boundary condition in all directions. Time history of bubble shape is illustrated in Figure 6 in comparison with the results of Jain et al [46].A similar problem for merging droplets is also analyzed, in which two droplets with similar conditions to Xing et al [47] are released next to each other. Time history of the droplet geometry in merging process is depicted in Figure 7 and is in good agreement with results of Xing et al [47].

Changes of summation of composition variables in time are shown in Figure 8, which demonstrates mass conservation and convergence of the model for merging bubbles and droplets test cases.

3.1.3. Single Rising Bubble

Rising of a single bubble due to gravity was simulated in the previous validation test case. As mentioned in the Introduction section, research of Bhaga and Weber [2] is one of the basic references in this area, and is usually referred to for verification of numerical analyses of single rising bubble, where several conditions of non-dimensional numbers have been tested. In this sub-section, four different conditions are selected, analyzed, and compared as illustrated in Figure 9. Bubble diameter and mesh size are 40 and 160×200 lattice unit, respectively.

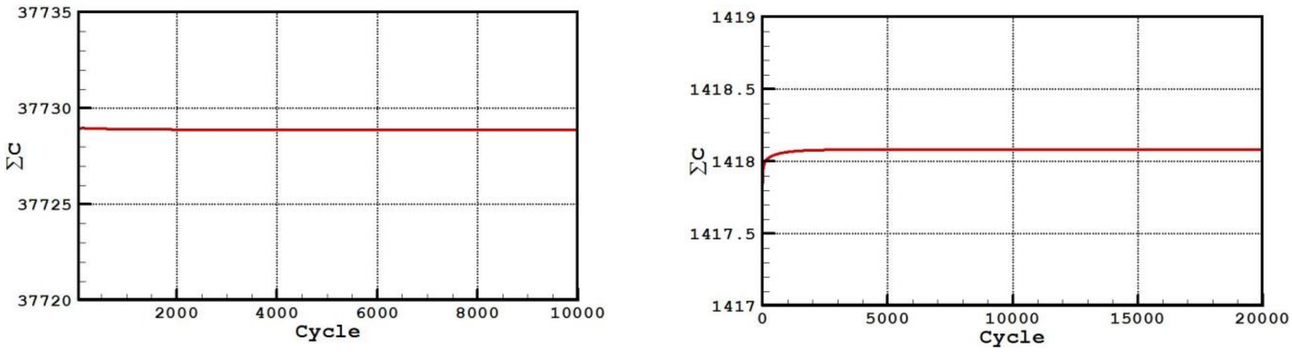

(a) (b)

Figure 8. Summation of composition vs. time for merging bubbles (a) and merging droplets (b)

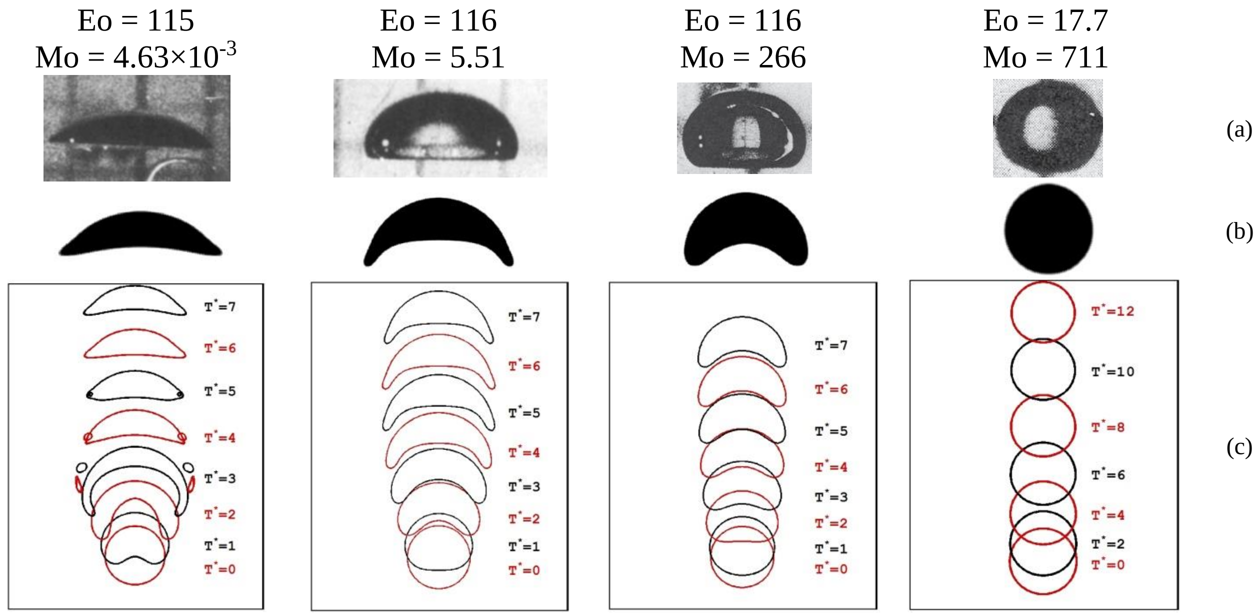

Figure 9. Shapes of rising bubble at different Eotvos and Morton numbers. (a) bubble shape in experiments of Bhaga and Weber [2], (b) final bubble shape in present study and (c) time history of bubble shape from stationary state (present study).

As can be seen in Figure 9, there is a good agreement between results of two-dimensional simulations with experimental results; this, along with the massive amount of researches in literature in which bubble dynamics has been investigated using two-dimensional analyses, show that two-dimensional simulation of bubbles can be reliable to some extent.

3.2. Two Rising Bubbles

In this section, rising and merging of two bubbles is simulated with 2, 10 and 50 Eotvos numbers. Diameter of bubbles is 50 lattice units in all three simulations, computational domain is 200×500, and boundary condition in all walls is periodic. Density, viscosity and gravity are constant in all three simulations and difference in Eotvos numbers is created by changing surface tension. Important variables in this problem are summarized in Table 1. Specific time in a rising bubble problem is defined as $\bar{T} = \sqrt{d/g}$, which in this study is equal to 3162 time unit (tu). Non-dimensional time is calculated as below.

$$T^* = \frac{T}{\bar{T}} \tag{27}$$

Bubbles are released at the center of domain width, at two heights of 40 and 120. Rising movement, deformation, and merging of bubbles until the non-dimensional time T*=10 are illustrated in Figures 10, 11, and 12, respectively for Eotvos numbers of 2, 10, and 50.

Table 1. Values of main variables in simulation of two bubble dynamics

variable	symbol	unit	value
liquid density	ρ_l	mu/lu3	1
bubble density	ρ_g	mu/lu3	0.1
liquid viscosity	μ_l	mu/(lu.tu)	0.1
bubble viscosity	μ_g	mu/(lu.tu)	0.01
gravity	g	lu/tu2	5×10-6
surface tension	σ	mu/tu2	0.005625, 0.001125, 0.000225
Eotvos number	Eo	-	2, 10, 50
Morton number	Mo	-	0.0025, 0.316, 39.5
bubble diameter	d	lu	50
specific time	$\bar{T}$	tu	3162

Bubbles are released at the center of domain width, at two heights of 40 and 120. Rising movement, deformation, and merging of bubbles until the non-dimensional time T*=10 are illustrated in Figures 10, 11, and 12, respectively for Eotvos numbers of 2, 10, and 50.

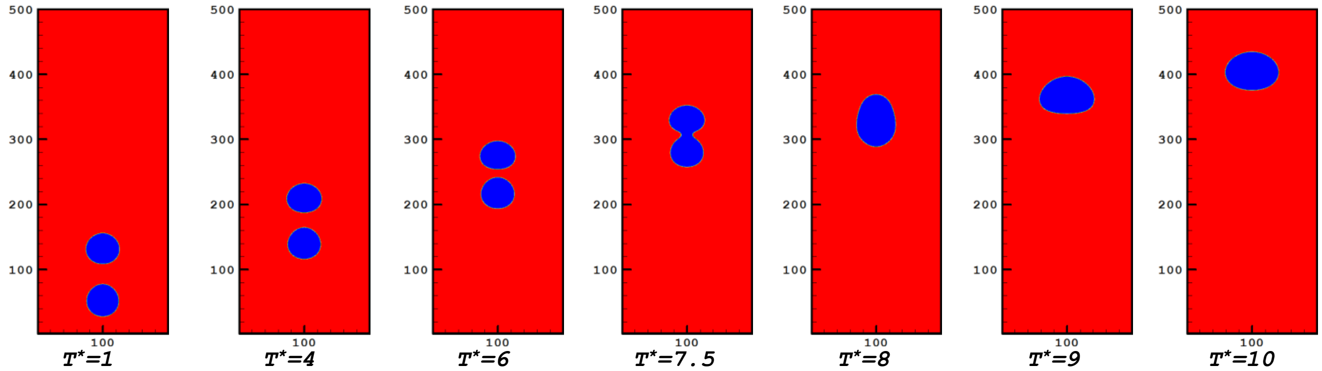

Figure 10. Rising and coalescence of two bubbles with Eotvos number 2 (Eo = 2)

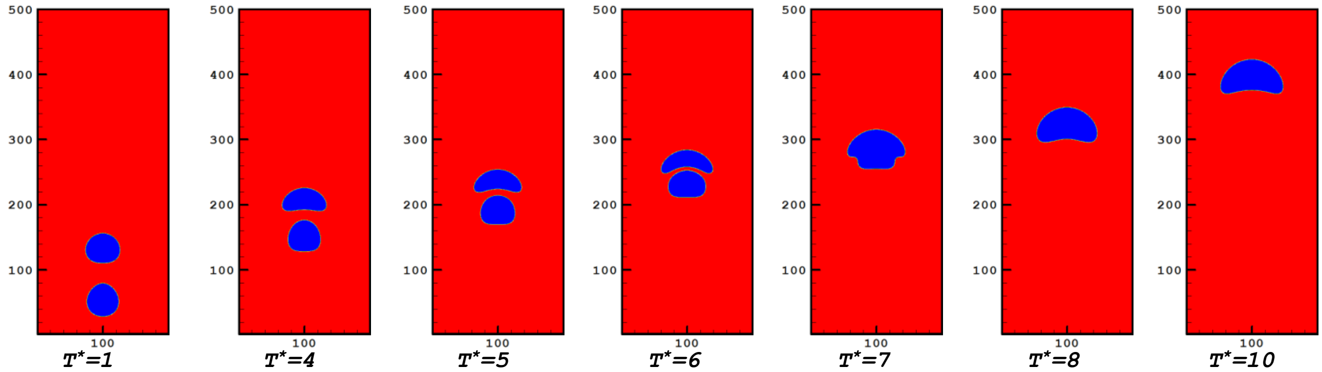

Figure 11. Rising and coalescence of two bubbles with Eotvos number 10 (Eo = 10)

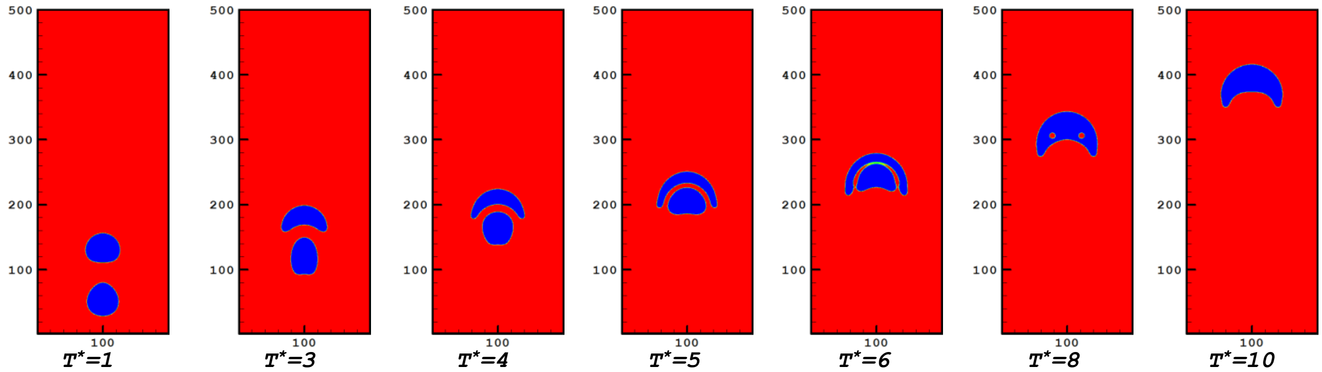

Figure 12. Rising and coalescence of two bubbles with Eotvos number 50 (Eo = 50)

In all the three conditions, the lower bubble, which is within the wake region of the upper one, is absorbed by and merged with the upper bubble. At lower Eotvos numbers, tendency to deformation is low and bubbles are in oval shapes before and after merging. However at larger Eotvos numbers, the effect of surface tension force decreases and does not have the required capability to preserve the circular shape of the bubble. Therefore, the deformation of the bubbles is much greater and the merged bubble is in curved shape.

3.3. Simulation of a Set of Nine Rising Bubbles

In this section, dynamics of rising motion of a set of nine bubbles due to gravity is simulated for two square and lozenge configurations and at three Eotvos numbers of 2, 10, and 50. Bubbles are released in a circular shape, with a 1.5d center-to-center distance. Computational domain is 400×1000 and initial diameter of bubbles is 50 lattice unit. Rising, deformation and merging of bubbles with square and lozenge configurations and 2 and 10 Eotvos numbers are illustrated in Figures 13, 14, 15 and 16.

In square configuration, three columns of bubbles slightly push each other away. Then, two upper bubbles of each column merge and the lower bubble pursues the upper one. Finally, bubbles of the middle column surpass other columns.

As demonstrated in Figure 15, at Eotvos number of 10, bubbles of each column in square configuration merge with each other and the resulted three bigger bubbles are observed in the domain. As time passes, the square layout collapses and the bubbles form a triangle arrangement resembling a tip of an arrow. A similar phenomenon can be seen in lozenge configuration. In this configuration, a leading bubble is present, which remains at the lead all the time. The first combination usually involves the two side bubbles, each of which merges with its bottom bubble. The leading bubble as well merges with the central one, although far from it.

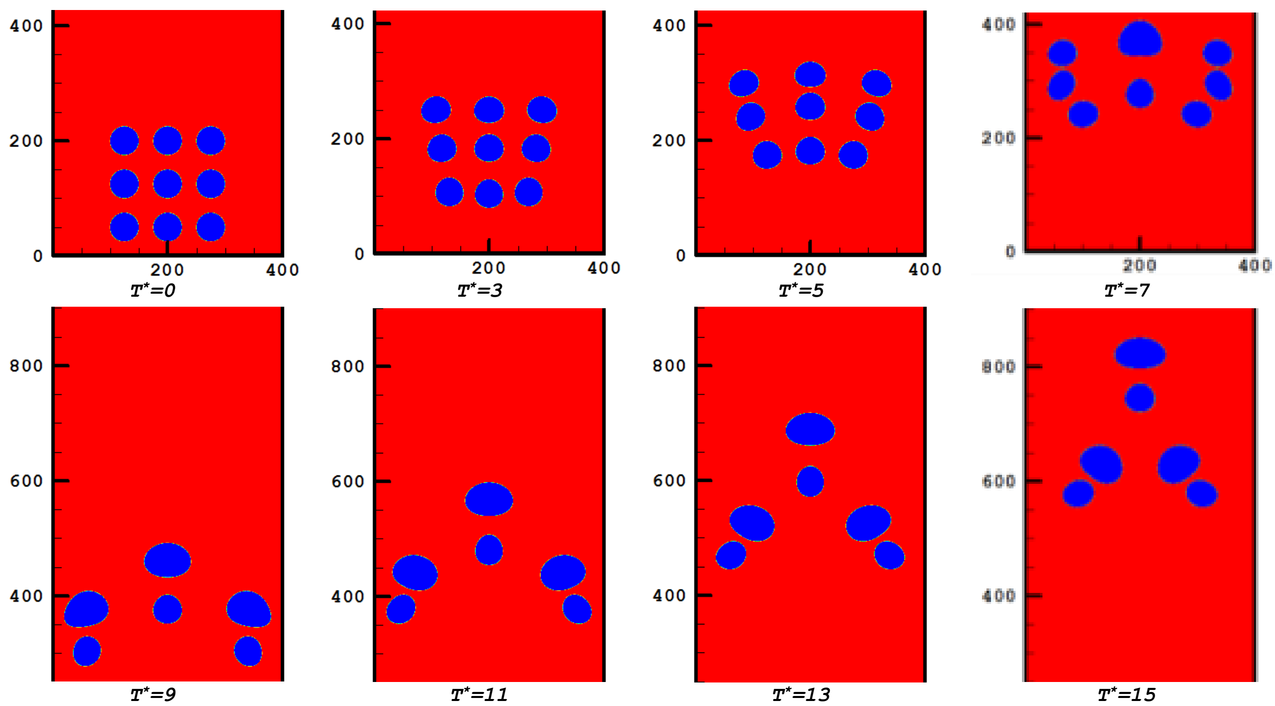

Figure 13. Dynamics and deformation of 9 rising bubbles with square configuration and Eotvos number 2 (Eo = 2)

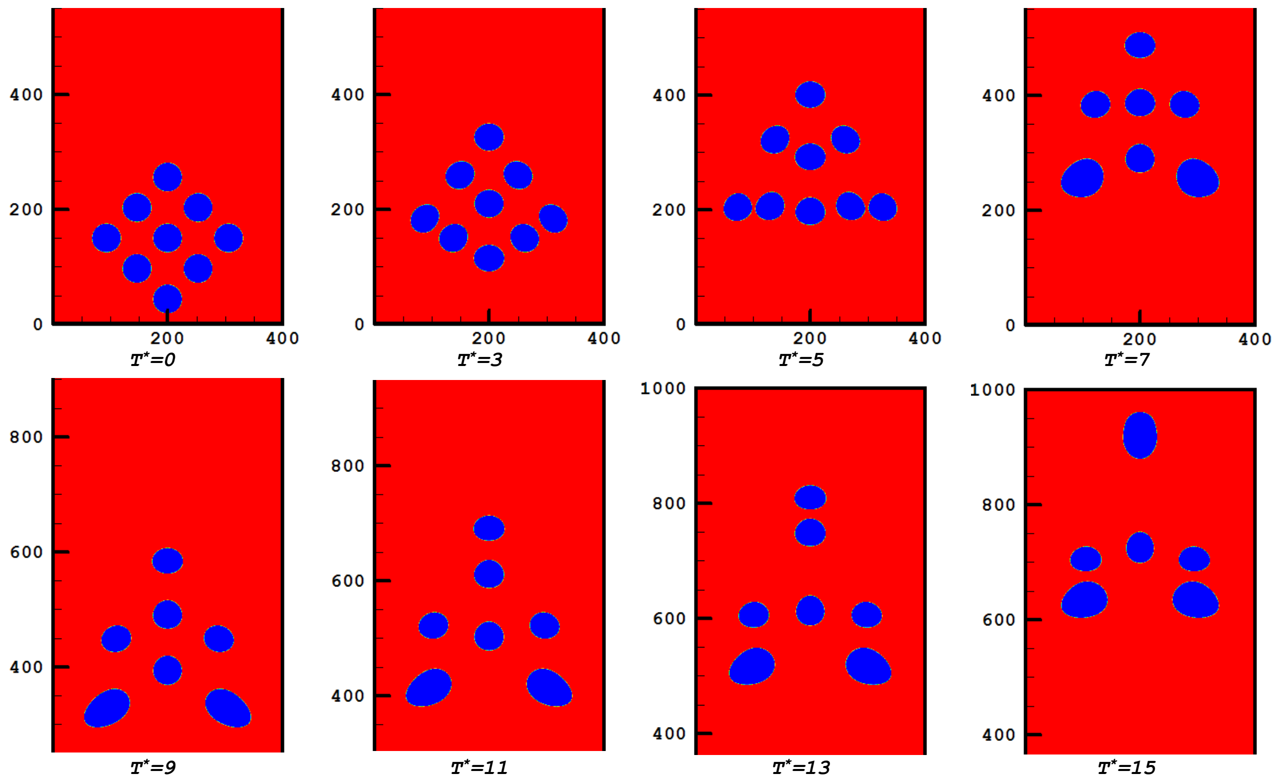

Figure 14. Dynamics and deformation of 9 rising bubbles with lozenge configuration and Eotvos number 2 (Eo = 2)

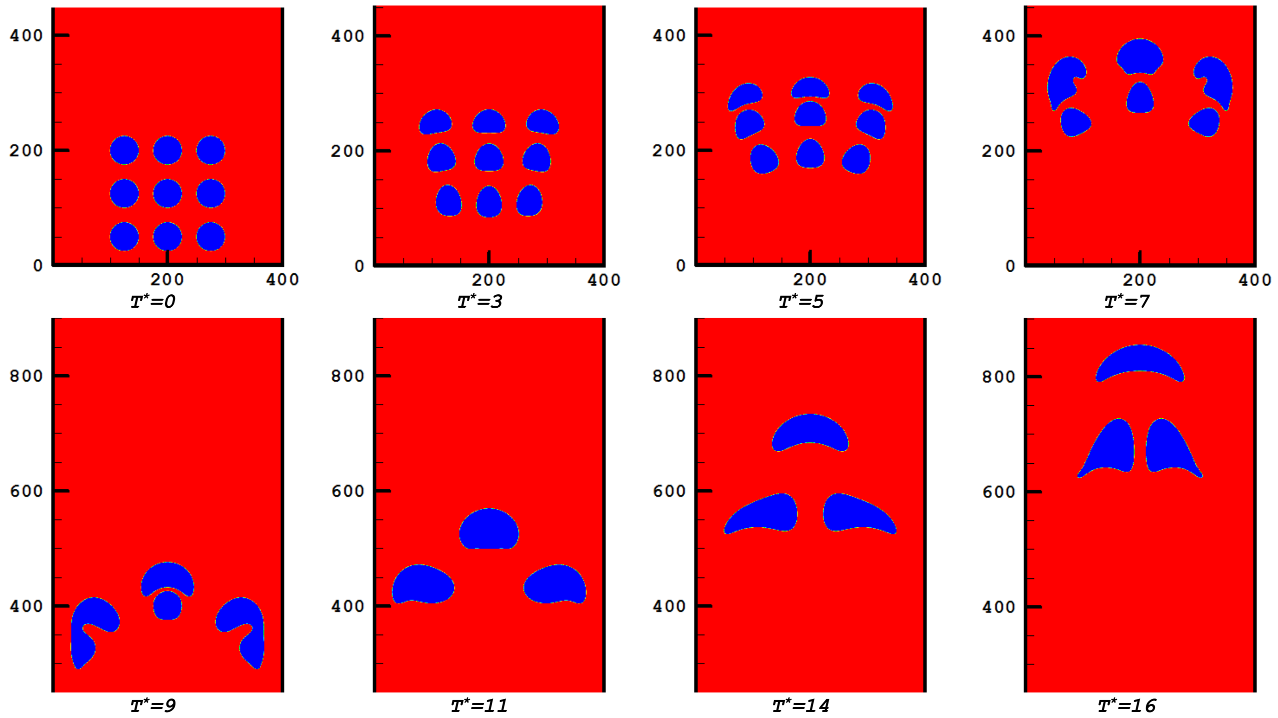

Figure 15. Dynamics and Deformation of 9 Rising Bubbles with Square Configuration and Eotvos Number 10 (Eo = 10)

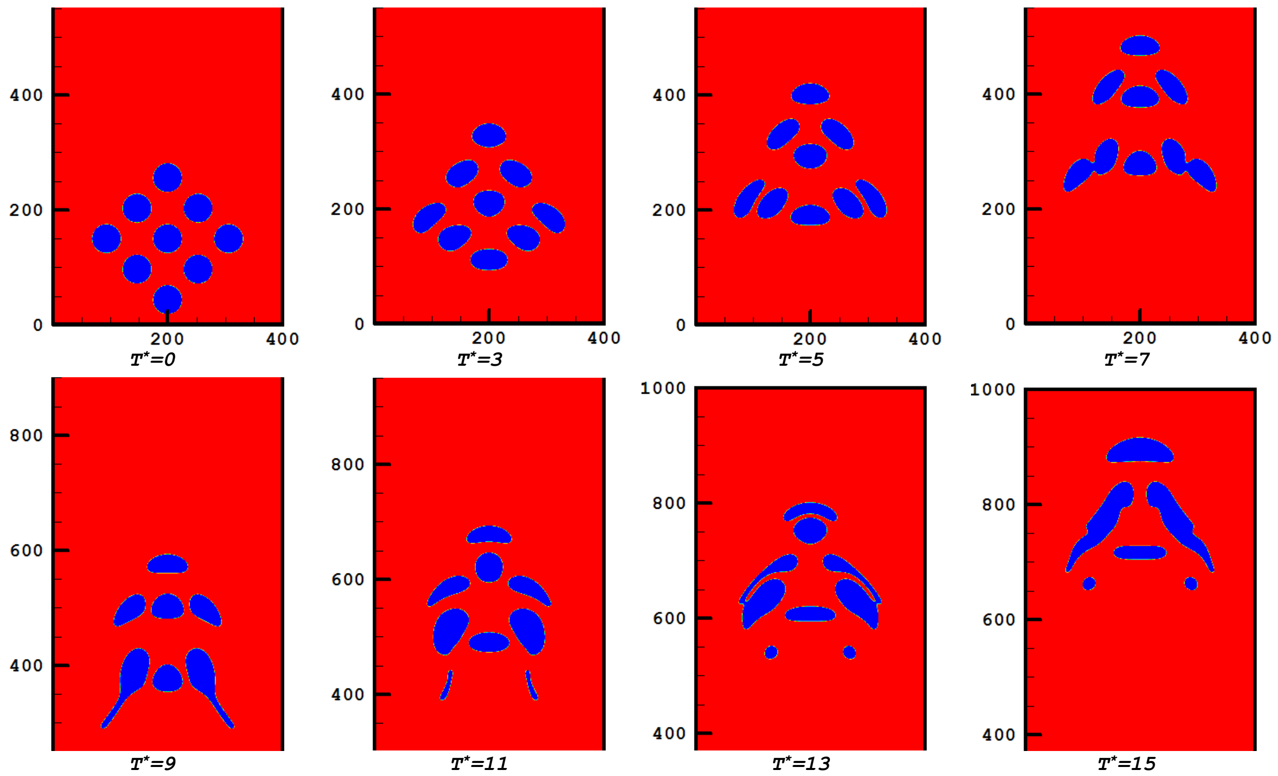

Figure 16. Dynamics and Deformation of 9 Rising Bubbles with Lozenge Configuration and Eotvos Number 10 (Eo = 10)

Velocity field of a set of nine bubbles with lozenge configuration, Eotvos number of 10, and non-dimensional times of 6, 9, 12 and 15 is depicted in Fig. 17. At the left column of this Fig., velocity magnitude is illustrated, where the velocity of the bubble set increases with time. As can be seen In the graph for non-dimensional time of 9, the two side bubbles combined have a higher velocity compared to the other ones. It can be concluded that for the bubbles larger in size, the buoyancy force is more likely to dominate the drag force, and thus to accelerate the upward movement of the bubble.

In the graphs for non-dimensional times of 12 and 15, as the bubble set moves upward, a wake is formed behind the set, which moves upwards with an equal velocity to the climbing velocity of the bubble set. With a deeper look at the two graphs, it can be seen that the velocity of the upstream fluid behind the bubble set is somewhat higher than the velocity of the lower bubbles and the flow velocity in the space between the bubbles, which can be considered as a responsible factor in pushing the lower bubbles towards the leading ones and merging them.

In graphs on the right side of Fig. 17, the streamlines are shown at the corresponding times with the left-hand graphs. The most striking feature of these graphs is the vortices formed on both sides of the bubble set. The existence of these vortices is necessary for the mass conservation in computational domain. In other words, the ascension of the fluid in the wake behind the bubble set is offset by downward moving of the fluid located far away from the bubble set. With this description, it seems that the shape of these vortices depends on the width of the domain; in other words, it is expected that with an increase in the domain width, larger but weaker vortices would form at the bubble set sides.

Finally, the deformation and merging of bubbles in the upward movement of the bubble set with square and lozenge configurations and Eotvos number of 50 are shown in Figures 18 and 19. The general pattern of rising and merging is almost similar to lower Eotvos numbers; but, as in the case of two bubbles, the effect of the surface tension force decreases at higher Eotvos numbers; therefore, the deformation of the bubbles is more intense and interesting shapes are noticed for the combination of bubbles.

4. Conclusion

Lee model is one of the most powerful models in simulation of two-phase flow with lattice Boltzmann method, which was used in this paper to study the dynamics of a rising bubble set for the first time. Two initial configurations of square and lozenge for a set of nine bubbles were considered and each was studied for three Eotvos numbers of 2, 10 and 50.

According to the Simulations, the overall behavior for the square arrangement of bubbles can be summarized as follows. As indicated, the three bubble columns take some distance from each other initially. Then, the two upper bubbles of each column are combined and the lower bubble of each column is pulled by the merged bubbles; and the middle column always moves faster than the adjacent columns.

In the lozenge configuration and for low and medium Eotvos numbers (Eo = 2 and Eo = 10), the first integration usually involves the two lateral bubbles, each of which merges with the bottom bubbles. The leading bubble is also combined with the central bubble, although far from it. At higher Eotvos numbers (Eo = 50), the effect of surface tension force decreases; therefore, the deformation of the bubbles is more intense and interesting shapes of merging bubbles were observed.

During the simulations of the rising bubble set, it was also noticed that with the upward movement of the bubble set, a wake of fluid is formed behind the bubble set. This wake moves upward, so that the fluid flow velocity behind the bubble set is somewhat higher than the velocity of the lower bubbles and the flow velocity in the space between the bubbles. This phenomenon can be considered as the responsible factor in pushing the lower bubbles towards the leading ones and merging them.

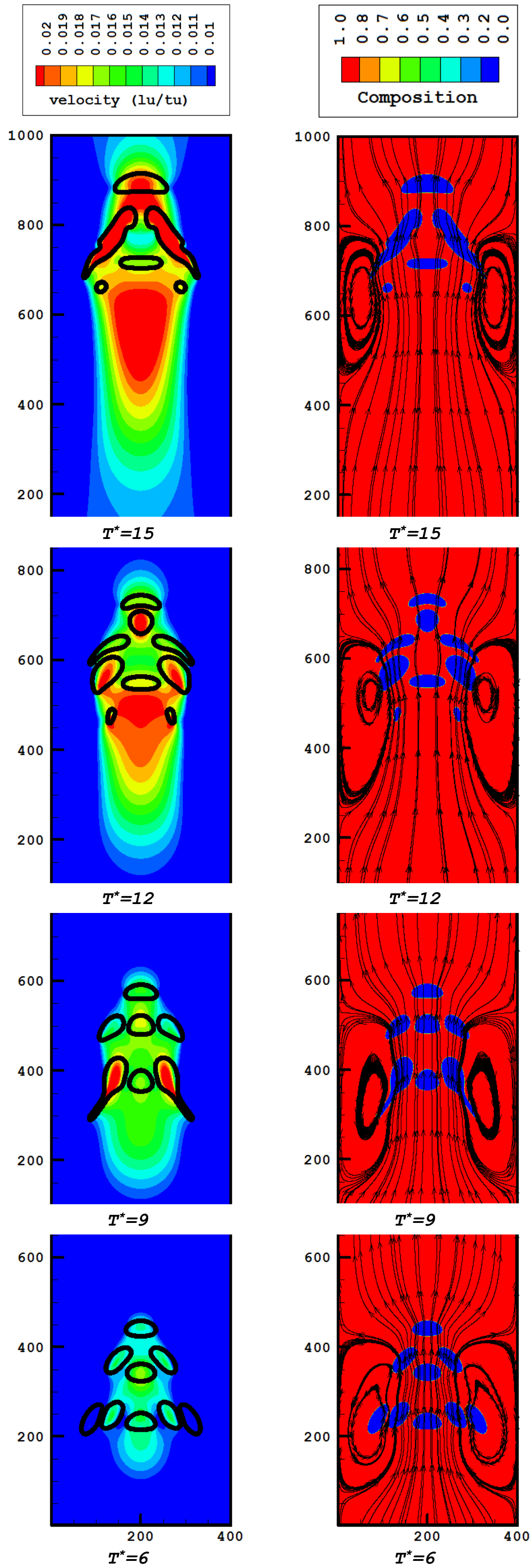

Figure 17. Velocity Distribution of 9 Rising Bubbles with Lozenge Configuration and Eotvos Number 10 (Eo = 10)

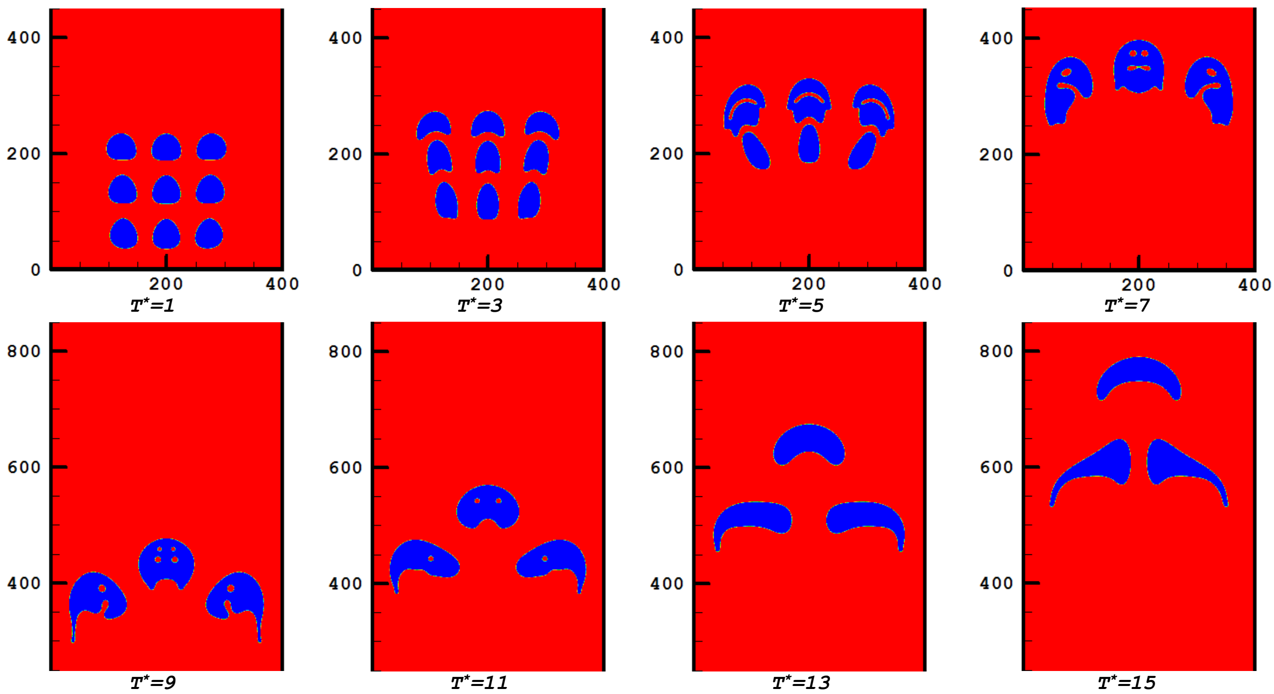

Fig. 18 Dynamics and Deformation of 9 Rising Bubbles with Square Configuration and Eotvos Number 50 (Eo = 50)

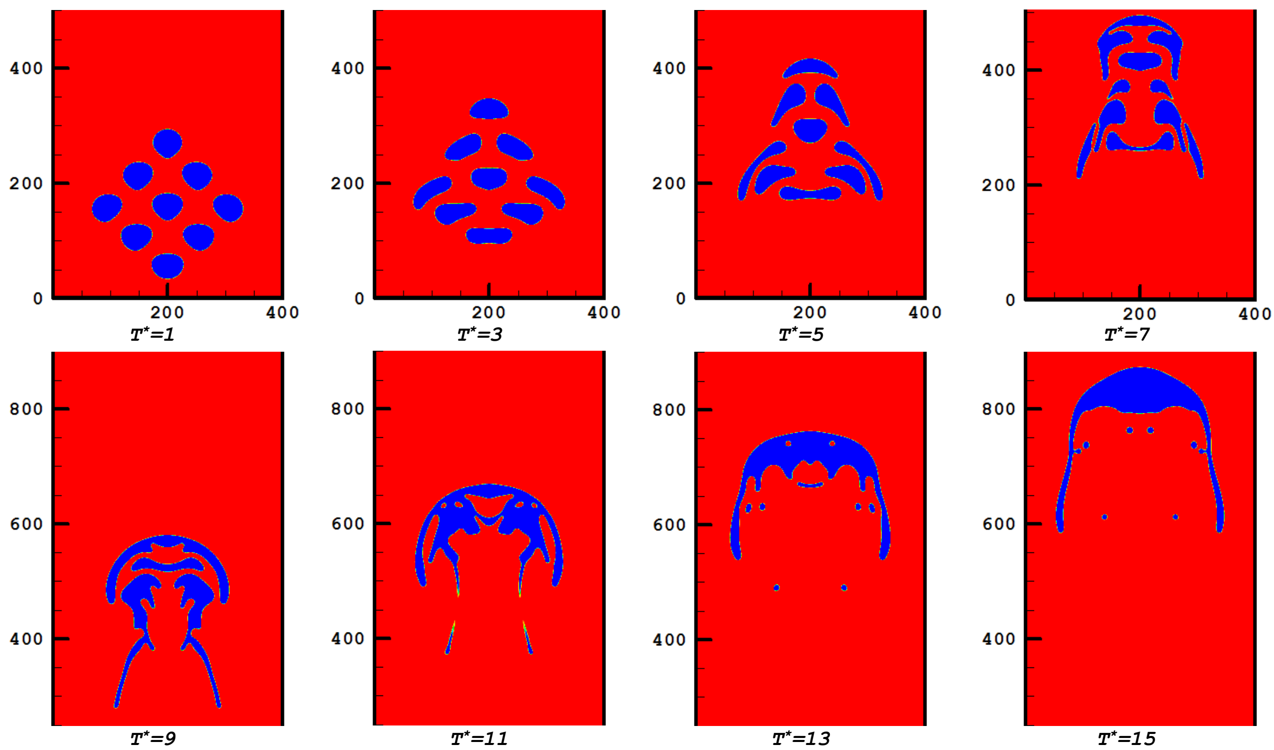

Fig. 19 Dynamics and Deformation of 9 Rising Bubbles with Lozenge Configuration and Eotvos Number 50 (Eo = 50)

References

1. Clift R., Grace J.R., 1978, Weber M.E., Bubbles, drops, and particles, New York: Academic Press.
2. Bhaga D., Weber M.E., 1981, Bubbles in viscous liquids: shapes, wakes and velocities, J Fluid Mech 105: 61-85.
3. Grace J.R., Wairegi T., Nguyen T.H., 1976, Shapes and velocities of single drops and bubbles moving freely through immiscible liquids, Trans. Inst. Chem. Eng 54(3): 167-173.
4. Watanabe H., Suzuki M., Ito N., 2013, Huge-scale molecular dynamics simulation of multibubble nuclei, Computer Physics Communications 184(12): 2775-2784.
5. Balcázar N., Lehmkuhl O., Jofre L., Oliva A., 2015, Level-set simulations of buoyancy-driven motion of single and multiple bubbles, International Journal of Heat and Fluid Flow 56: 91-107.
6. Islam M.T., Ganesan P., Cheng J., 2015, A pair of bubbles' rising dynamics in a xanthan gum solution: a CFD study, Rsc Advances 5(11): 7819-7831.

7. Hassanzadeh A., Pourmahmoud N., Dadvand A., 2017, Numerical simulation of motion and deformation of healthy and sick red blood cell through a constricted vessel using hybrid lattice Boltzmann-immersed boundary method, Computer methods in Biomechanics and Biomedical engineering 20(7): 737–749.
8. Hassanzadeh A., Pourmahmoud N., Dadvand A., 2018, Numerical simulation of red blood cell motion and deformation using improved lattice Boltzmann-immersed boundary method", Iran J Sci Technol Trans Mech Eng, (In Press), DOI 10.1007/s40997-017-0112-2.
9. Ghafouri A., Hassanzadeh A., 2017, Numerical study of red blood cell motion and deformation through a michrochannel using lattice Boltzmann-immersed boundary method. Journal of the Brazilian Society of Mechanical Sciences and Engineering, 39(6): 1873-1882.
10. Dadvand A., 2016, Simulation of the motion of two elastic membranes in Poiseuille shear flow via a combined immersed boundary-lattice Boltzmann method. Journal of Computational Science 12: 51-61.
11. Dadvand A., 2018, Effects of deformability of RBCs on their dynamics and blood flow passing through a stenosed microvessel: an immersed boundary-lattice Boltzmann approach, Theoretical and Computational Fluid Dynamics, 32(1): 91-107.
12. Gunstensen K., Rothman D.H., Zaleski S., Zanetti G., 1991, Lattice Boltzmann model of immiscible fluids, Physical Review A 43(8): p. 4320.
13. Grunau D., Chen S., Eggert K., 1993, A lattice Boltzmann model for multiphase fluid flows, Phys. Fluids A 5(10): p. 2557.
14. Shan X., Chen H., 1993, Lattice Boltzmann model for simulating flows with multiple phases and components, Phys. Rev. E 47(3): p. 1815.
15. Shan X., Chen H., 1994, Simulation of non-ideal gases and liquid–gas phase transitions by the lattice Boltzmann equation, Phys. Rev. E 49: p. 2941.
16. Shan X., Doolen G.D., 1995, Multicomponent lattice-Boltzmann model with interparticle interaction, J. Stat. Phys. 81: 379-393.
17. Shan X., Doolen G., 1996, Diffusion in a multicomponent lattice Boltzmann equation model, Phys. Rev. E 54(4): p. 3614.
18. Swift M.R., Osborn W.R., Yeomans J.M., 1995, Lattice Boltzmann simulation of nonideal fluids, Phys. Rev. Lett. 75(5): p. 830.
19. Swift M.R., Orlandini E., Osborn W.R., Yeomans J.M., 1996, Lattice Boltzmann simulation of liquid–gas and binary-fluid system, Phys. Rev. E 54(5): p. 5041.
20. Orlandini E., Swift M.R., Yeomans J.R., 1995, A Lattice Boltzmann Model of Binary-Fluid Mixtures, Europhys. Lett. 32 (6): 463-468.
21. He X., Shan X., Doolen G.D., 1998, A discrete Boltzmann equation model for non-ideal gases, Phys. Rev. E 57(1): p. R13.
22. He X., Chen S., 1999, Zhang R., A lattice Boltzmann scheme for incompressible multiphase flow and its application in simulation of Rayleigh–Taylor instability, J. Comput. Phys. 152(2): 642–663.
23. He X., Zhang R., Chen S., Doolen G.D., 1999, On three-dimensional Rayleigh– Taylor instability, Phys. Fluids 11(5): p. 1143.
24. Zhang R., He X., Chen S., 2000, Interface and surface tension in incompressible lattice Boltzmann multiphase model, Comput. Phys. Commun. 129: 121–130.
25. Zhang R., He X., Doolen G., Chen S., 2001, Surface tension effects on two-dimensional two-phase Kelvin-Helmholtz instabilities, Advances in Water Resources 24: 461-478.
26. Zhang R., 2000, Lattice Boltzmann approach for immiscible multiphase flow, Ph.D. thesis, University of Delaware.
27. Inamuro T., Ogata T., Tajima S., Konishi N., 2004, lattice Boltzmann method for incompressible two-phase flows with large density differences, J. Com. Phy.198: 628–644.
28. Lee T., Lin C.L., 2005, A stable discretization of the lattice Boltzmann equation for simulation of in compressible two-phase flows at high density ratio, J. Com. Phy. 206: 16–47.
29. Zheng H.W., Shu C., Chew Y.T., 2006, A lattice Boltzmann for multiphase flows with large density ratio, J. Com. Phy. 218: 353–371.
30. Takada N., Misawa M., A. Tomiyama, S. Hosokawa, 2001, Simulation of bubble motion under gravity by lattice Boltzmann method, Journal of Nuclear Science and Technology 38(5): 330–341.
31. Gupta A., Kumar R., 2008, Lattice Boltzmann simulation to study multiple bubble dynamics, International Journal of Heat and Mass Transfer 51(21-22): 5192–5203.
32. Cheng M., Hua J., Lou J., 2010, Simulation of bubble–bubble interaction using a lattice Boltzmann method, Computers & Fluids 39: 260–270.
33. Yu Z., Yang H., Fan L.S., 2011, Numerical simulation of bubble interactions using an adaptive lattice Boltzmann method, Chemical Engineering Science 66(14): 3441–3451.
34. Shu S., Yang N., 2013, Direct Numerical Simulation of Bubble Dynamics Using Phase-Field Model and Lattice Boltzmann Method, Industrial & Engineering Chemistry Research 52: 11391−11403.
35. Lee T., Fischer P.F., 2006, Eliminating parasitic currents in the lattice Boltzmann equation method for nonideal gases, Phys. Rev. E 74: No. 046709.
36. Lee T., Liu L., 2008, Wall boundary conditions in the lattice Boltzmann equation method for non-ideal gases, Physical Review E 78: No. 017702.
37. Lee T., 2009, Effects of incompressibility on the elimination of parasitic currents in the lattice Boltzmann equation method for binary fluids, Comput. Math. Appl. 58: 987–994.
38. Lee T., Liu L., 2010, Lattice Boltzmann simulations of micron-scale drop impact on dry surfaces, J. Com. Phy. 229: 8045-8063.
39. Amaya-Bower L., Lee T., 2010, Single bubble rising dynamics for moderate Reynolds number using Lattice Boltzmann Method, Computers & Fluids 39: 1191–1207.
40. Amaya-Bower L., Lee T., 2011, Numerical simulation of single bubble rising in vertical and inclined square channel using lattice Boltzmann method, Chemical Engineering Science 66: 935–952.
41. Taghilou M., Rahimian M.H., 2014, Investigation of two-phase flow in porous media using lattice Boltzmann method, Computers and Mathematics with Applications 67: 424–436.
42. Mirzaie Daryan H.M., Rahimian M.H., 2015, Numerical Simulation of Single Bubble Deformation in Straight Duct and 90˚ Bend Using Lattice Boltzmann Method, Journal of Electronics Cooling and Thermal Control 5: 89-118.
43. Haghani R., Rahimian M.H., 2016, Four different types of a single drop dripping down a hole under gravity by lattice Boltzmann method, Journal of Computational Applied Mechanics 47(1): 89-98.
44. Farokhirad S., Morris J.F., Lee T., 2015, Coalescence-induced jumping of droplet: Inertia and viscosity effects, Physics of Fluids 27(10).

45. Fakhari A., Bolster D., 2017, Diffuse interface modeling of three-phase contact line dynamics on curved boundaries: A lattice Boltzmann model for large density and viscosity ratios. Journal of Computational Physics 334: 620-638.
46. Jain P.K., A. Tentner, Rizwan-uddin, 2009, A lattice Boltzmann framework to simulate boiling water reactor core hydrodynamics, Computers and Mathematics with Applications 58: 975-986.
47. Xing X.Q., Butler D.L., Ng S.H., Wang Z., Danyluk S., Yang C., 2007, Simulation of droplet formation and coalescence using lattice Boltzmann-based single-phase model, Journal of Colloid and Interface Science 311: 609–618.